TECHNICAL PAPER

CrossMark

Investigation of hole quality in rotary ultrasonic drilling of borosilicate glass using RSM

Vikas Kumar[1] · Hari Singh[1]

Abstract
The present article emphasizes on reducing the edge chipping and taper during rotary ultrasonic drilling of one of the most demanded ceramic glasses "BK-7." Statistical tools of design of experiments and backing plate were adopted as two distinct approaches to curb the chipping damage. Central composite design has been conjugated with desirability function for framing the design matrix. This investigation also emphasizes to study the effect of process variables—spindle speed, ultrasonic power and feed rate—on the chipping width (CW) and taper (T). After developing the second-order regression models for the CW and T, analysis of variance was used to check the fitness of regression models and recognizing the significant model terms. Then impact of each process parameter was analyzed on responses of interest through 3-D surface plots. The feed rate came forth as the most dominating factor by having maximum influence over the qualitative aspects "CW" and "T" of the drilling process. Interactions of higher rpm and power with lower feed effectively reduced the CW and T. The backing material, employed during main experimentation, also proved its effectiveness to reduce CW when main experiments results were compared to the results of pilot experimentation, which was performed without backing plate. Scanning electron microscope (SEM) was used to analyze the different tool wear modes and microstructure of machined surfaces. Tool weight measurement revealed the dominance of bond fracture and grain fracture during the early stage of the drilling process. Apart from brittle fracture, SEM also affirmed the presence of plastically deformed regions over the machined surfaces. Little deviations between the predicted values and experimental values during the confirmatory tests validated the prediction accuracy of regression models at 95% confidence level.

Keywords Chipping · Taper · Optimization · RSM · Desirability · Wear · Ultrasonic · Drilling

1 Introduction

BK7 is borosilicate crown glass having homogeneous and bubble-free structure with low inclusion content. It is endowed with a superlative combination of optical and mechanical properties. Moreover, it possesses the chemical stability and high resistance to thermal shocks due to its low coefficient of thermal expansion. Owing to these characteristics, BK7 is finding numerous applications in

manufacturing sectors to fabricate MEMS, mirrors, prisms, lenses, electronic substrates, microfluidic devices, laboratory equipment, polarizers, etc., and is considered as a reference glass for other optical glasses. Due to low refractive index, BK7 is also used to make the doublet lens with flint glasses to prevent the chromatic aberration [1–4].

However, fabrication of BK7 has been always been a tough task for process engineers owing to its high hardness and low fracture toughness. Machining the glasses by conventional machining methods and alternative non-traditional machining methods like laser machining and abrasive water jet machining have the shortcomings like higher cutting forces, stray cutting, high tool wear rate, large kerf width, severe surface degradation, etc. [5, 6]. Ultrasonic machining (USM) has been extensively used for fabrication of glasses and other clans of brittle materials. However, low material removal rate (MRR), low aspect ratio, higher cutting forces are some of the practical barriers of USM, which demand

Technical Editor: Márcio Bacci da Silva, Ph.D.

✉ Vikas Kumar
  vikas.thermal@gmail.com

  Hari Singh
  hsingh_nitk@rediffmail.com

1 Mechanical Engineering Department, National Institute of Technology, Kurukshetra, Kurukshetra, India

a more realistic machining solution [7]. Rotary ultrasonic machining (RUM) is emerging as a strong competitor to USM as it exhibits 6–10 times higher MRR comparative to USM, that too with low cutting forces, less tool wear and superior surface characteristics [8–10].

Often RUM is considered as up-gradation of USM. However, RUM is distinct from USM in many ways. Firstly, abrasives are coated over tool and there is no involvement of slurry like USM. Secondly, other than feed motion and ultrasonic vibrations, tool is also given the rotational motion [11]. Under the combined influence of these three different motions of tool—feed motion (longitudinal or lateral), rotational motion and ultrasonic vibration—the abrasives follow either sinusoidal trajectory (as in case of grinding and milling when tool moves parallel to work surface) or spiral sinusoidal trajectory (when tool moves perpendicular to workpiece surface as in case of drilling). The additional motion, i.e., rotation of tool in RUM makes it superior to USM in material removal mechanism [8, 12]. Furthermore, Unlike USM (where there is no direct contact between workpiece and tool), tool in RUM has direct contact with the workpiece through abrasives coated over it. Therefore, RUM is an advanced machining process rather than non-traditional machining process like USM.

Due to the vast applications, BK7 glass frequently undergoes drilling operation. Then these drilled parts need to be assembled to main product. The quality of assembly depends directly over the hole quality indexes like edge quality, taper and surface characteristics of machined surface. Measuring the chipping damage (breaking of edges of hole) is common practice in drilling for accessing the hole quality. Therefore, it becomes vital to reduce the chipping as well as taper. Failure, to minimize these quality parameters, will lead to poor precision of assembly and performance degradation of product during its service life. Therefore, BK-7 was drilled by RUM, which is termed as rotary ultrasonic drilling (RUD). The focus of study is to access the hole quality and machining performance in terms of edge chipping and taper.

Research studies available on RUM were reviewed critically to identify some more gaps. In a recent study, Jain et al. [13] performed peck drilling of brittle materials that are used in aerospace applications. Authors used tools with different wall thickness and grain size. Tools having lower thickness and fine grains produced minimum chipping area and taper due to significant reduction in cutting forces. Sharma et al. [14] proposed a mathematical model to measure the chipping damage in terms of its volume. Authors also inferred that tool wear is greatly dependent on surface area of tool, which is in contact with workpiece. Song et al. [15] machined dental ceramic with and without using ultrasonic vibrations. Use of ultrasonic vibrations was postulated to prevent the premature failure of dental restoration due to consistent and significant reduction in chipping damage

and subsurface damage. Jain et al. [16] opted for measuring the specific tool wear during microrotary ultrasonic drilling of borosilicate glass. Tool having high thickness with coarse grain reduced the tool wear, whereas it increased with increase in rotational speed. Wang et al. [17] used different tool configurations to curb the chipping damage in optical glasses. Out of these, compound tool suppressed the edge chipping to maximum extent due to reprocessing effect at hole exit and shielding of residual stresses at hole entrance. Lv [18] conducted rotary ultrasonic drilling of BK7 glass to correlate the kinematic behavior of abrasive with the generation of chipping at hole entrance. Authors reported that the trajectory of abrasive in RUD starts to approach to that of conventional drilling at higher rotational speed due to which beneficial effect of ultrasonic vibration on chipping diminishes.

Alam et al. [19] reported minimum damage to bone cells during ultrasonic drilling of bones comparative to conventional drilling. Authors also observed substantial increase in temperature with increase in rotational speed and feed of drill. Mandegari et al. [20] reported better hole quality in terms of circularity, cylindricity and surface finish with higher tool life in RUD of steel st304 in comparison with ultrasonic assisted drilling. Feng et al. [21] inferred high productivity with enhanced tool life in RUD of carbon fiber reinforced plastic (CFRP). All of the drilled holes were of almost similar size and possessed variability of only 1%. Churi et al. [22] performed RUD on Ti6Al4V using "one factor at a time (OFAT)" approach with the objective of observing the change in cutting force and surface finish with variation in process control factors. Higher feed rate was inferred to have obtrusive effect on the surface roughness due to generation of higher cutting forces. Zhao et al. [23] found remarkable reduction in cutting force during rotary ultrasonic grinding of optical glass K-9. Li et al. [24] compared the RUD of Ti6Al4V with conventional drilling (CD) in terms of burr height. RUD was reported as the superlative machining solution to produce holes with lower burr height. Gupta et al. [25] observed reduction in cutting force and torque during RUD of bones. Yuan et al. [26] performed rotary ultrasonic milling of C/SiC and T700 to develop chip size and chip space models to predict the tool blockage conditions. Wang [27] inferred reduction in chipping with newly designed conical drills in comparison with common drills. Kumaran et al. [12] inferred reduced burr at hole exit at the expense of increased thrust force in RUD of CFRP composite under low temperature conditions. Wang et al. [28] addressed the reduction in tearing size and drilling forces due to reprocessing effect of compound step drill during RUD of C/SiC. During RUD of quartz glass and sapphire, Wang et al. [29] reported 60% reduction in edge chipping with step drills having step thickness smaller than the thickness of drill end face. Wang et al. [30] performed RUD of

sapphire for validating the accuracy of predictions made by "chipping size" model based on K9 glass properties. Cong et al. [31] confirmed the superiority of RUD over other drilling methods with lower hole size variation and longer tool life by performing experiments on CFRP/Ti stacks.

Chipping in RUM is already seeking the attention of researchers. Different approaches have been adopted to suppress it like changing the feed rate at the end of drilling, changing the design and configuration of cutting tool and using the backing plate [7, 32, 33]. From the literature review, it is clear that no efforts have been made to control the chipping using statistical tools of design of experiments. The literature also explicates that little attention has been paid to the dimensional deviations like taper. Majority of research studies were performed at relatively narrow range of ultrasonic power (30–45%). Therefore, in the current study the range of ultrasonic power was broadened-up from 30 to 80% to analyze the process capability at higher power.

This study is focused on suppressing the chipping width (CW) and reducing the taper (T) for enhancing the hole quality during RUD of BK7. Central composite rotatable design (CCRD) of response surface methodology (RSM) was adopted for systematic planning of experimentation. Thereafter, analysis of variance (ANOVA) test was performed over experimental data to figure out the significance and percentage contribution of model terms. Then desirability function was used to find out the optimal parametric conditions to get the desired values of responses of interest. Effect of backing the material has also been studied over the chipping along with the tool wear pattern.

2 Experimental setup and methodology

Experimentation was performed on rotary ultrasonic machine (sonic mill, 1 kW). Figure 1 shows some of the key components of machine along with the magnified view of machining proximity. The working of RUM starts with the power supply of low-frequency electrical energy (50 Hz) that is amplified to high-frequency energy of the order of 20 kHz. In next stage, transducer (piezoelectric) converts the electrical energy into ultrasonic vibrations. However, the generated ultrasonic vibrations have lower order amplitude, which is amplified by the horn for effective machining. Spindle is driven by a motor, which controls the rotational speed of cutting tool. Flow of coolant is maintained through a coolant pump (centrifugal pump) to wipe-out the removed material from the machining zone.

Sintered diamond hollow core drills were used for drilling. The terminology of drill has been shown in Fig. 2. The specifications of tool are listed in Table 1. The tool also has two slots just opposite to each other for easy removal of microchips. The machine is designed to have a resonant
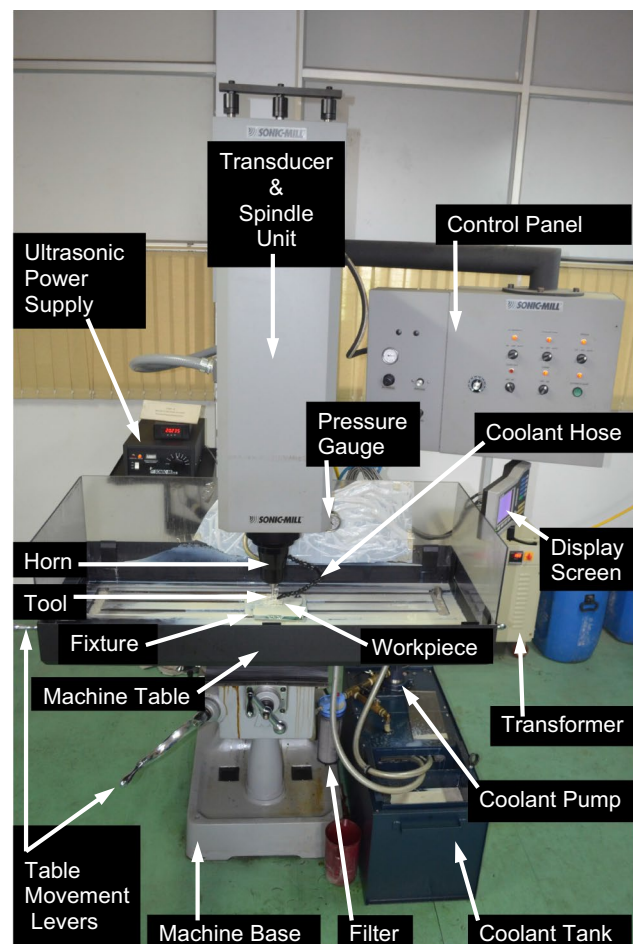

Fig. 1 Experimental setup of rotary ultrasonic drilling (RUD)

frequency of 20.43 ± 0.5 kHz in accordance with different weights and tuning lengths of the tool. The tuning length and weight of tool change the resonant frequency of the horn-tool assembly. In the current study, resonant frequency of tool having weight 28.1097 g and tuning length 57.30 mm was found to be 20.235 ± 0.05 kHz. Blasocut BC 20 SW cutting fluid mixed with deionized water in proportion of 1:18 (by volume) was used as the coolant media. The coolant pressure was kept constant at 30 lb per square inch (206.8 kPa).

Borosilicate crown glass BK-7 having dimensions 50 mm × 50 mm × 5 mm was used as the workpiece material. The composition of BK7 glass by weight includes 70% Silica, 11.5% boron oxide, 9.5% sodium oxide, 7.5% potassium oxide, 1% barium oxide and some other foreign elements [3]. The various properties of BK7 have been listed in Table 2.

2.1 Experimental procedure and data collection

From the results of pilot experiments, coolant pressure was found to have no impact over the responses of interest.
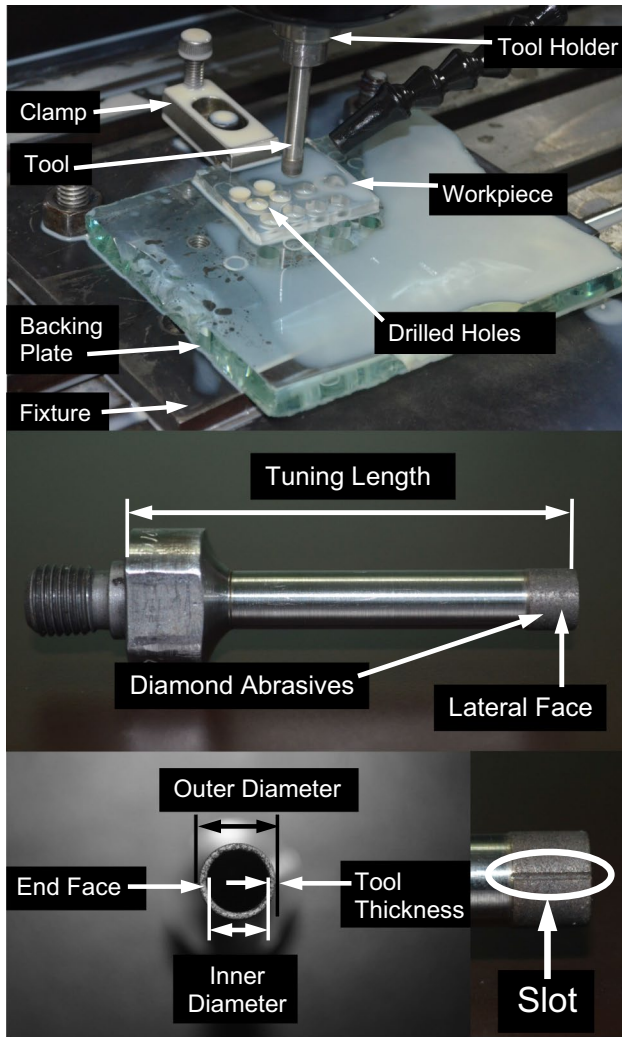
Fig. 2 Enlarged view of machining zone and tool features

Table 1 Tool specifications

Parameter	Value (unit)
Outer diameter	8 mm
Tool thickness	0.75 mm
Tool weight	28.1097 g
Tool bond	Metal binders
Tuning length	57.30 mm
Abrasive material	Diamond
Abrasive coating height	6.5 mm
Abrasive grade	220 mesh
Grit concentration	100
Binder	Metal
Slots	2 Slots
Fabrication	Sintering

Table 2 Properties of BK7 glass

Properties	Value	Unit
Abbe number	63.66	–
Refractive index	1.51	–
Coefficient of thermal expansion	7.1×10^{-6}	Per kelvin (up to 70 °C)
Density	2.51	g/cm^3
Fracture toughness	0.82	N/mm$^{3/2}$
Bulk modulus	34	GPa
Poisson's ratio	0.204	–
Young modulus	82	GPa
Knoop hardness	610	MPa
Softening point	719	°C
Vickers hardness	7.7×10^3	N/mm^2

So, it was excluded from final experimentation. Final experimental scheme included the three input variables namely feed rate, spindle speed and ultrasonic power. The details of input variables along with their levels are given in Table 3. The design expert software (Version 9.0) was used for framing the experimental matrix and statistical analysis of the experimental data.

In the present work, response surface methodology (RSM) has been employed for planning the experimentation. RSM is a set of statistical and mathematical tools that helps to analyze and model the problems with an objective to optimize a response, which is influenced by numerous process variables [34]. Central composite design of rotatable nature (CCRD) has been preferred over other designs of RSM to plan the experimentation as it possesses advantages like rotatability, high prediction accuracy and capability of estimating the curvature [35]. As the functional relationship between the responses of interest and input process variables was unknown, second-order polynomial equation was used to model the responses. Moreover, quadratic equations also estimate the curvature of responses. For more information about RSM and its design approaches, readers may refer book by Montgomery [36]. The quadratic equation for determining the responses in terms of input variables is:

$$R = \beta_0 + \sum_{i=1}^{k} \beta_i V_i + \sum_{i}^{k} \beta_{ii} V_i^2 + \sum_{i<j}^{k} \beta_{ij} V_i V_j \qquad (1)$$

where R denotes the desired output response, V_i denotes the process variables, k is the number of design variables, β_0, β_i, β_{ii}, β_{ij} are the regression coefficients.

CW and T have been considered to evaluate the quality of drilled hole. The tool makers microscope (SVI-IMG-3D,

Table 3 Input variables and their levels

Variables	Notation	Units	Levels				
			I	II	III	IV	V
Spindle speed	S	RPM	2318	3000	4000	5000	5682
Feed rate	F	mm/min	0.095	0.30	0.60	0.90	1.105
Ultrasonic power	P	%	30	40	55	70	80

Sipcon instrument industries, Ambala) was used for measuring the chipping contour and taper. Figure 3 embodies an illustration of the formation of edge chipping and some of the terms related to chipping nomenclature. Chipping width is calculated by taking the average of the difference between maximum diameter and hole diameter as given in Eq. 2.

$$CW = \frac{D_m - D_h}{2} \tag{2}$$

where D_m is the diameter of the circle concentric with drilled hole and passing through the extreme peak of chipping contour; D_h is the diameter of the drilled hole

Based on CCRD approach, three factors each with five levels resulted in 20 experimental settings that have been logged in Table 4 along with response values. The experimentation was replicated twice and final observation of response is the average of three measurements at same parametric setting.

3 Results and discussion

3.1 Response modeling

Experimental data summarized in Table 4 was subjected to regression analysis, and regression coefficients were estimated to develop the quadratic models for considered responses. The models were further modified by using the backward elimination technique which omits the insignificant model terms [37]. Regression coefficients corresponding to significant model terms were put into Eq. 1 and following regression equations were formulated for chipping width and taper.

Regression model for chipping width:

$$CW = 1.99927 + .00000993533\ S + 0.00175933\ F$$
$$- 0.0342377\ P - 0.00015875\ SF + 0.0108611\ FP$$
$$+ 0.695922\ F^2 + 0.000185659\ P^2 \tag{3}$$

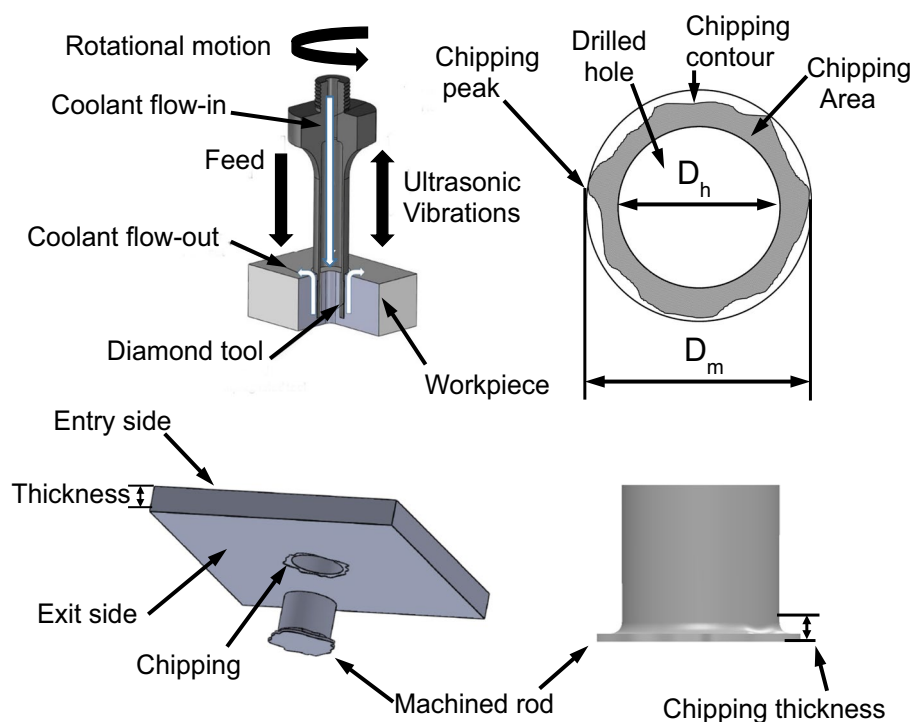**Fig. 3** Chipping formation illustration and chipping nomenclature

Table 4 Experimentation scheme with response observations

Trial number	Spindle speed (RPM)	Feed rate (mm/min)	Ultrasonic power (%)	CW (mm)	Taper degree
1	3000	0.3	40	1.019	0.483
2	5000	0.3	40	0.936	0.401
3	3000	0.9	40	1.476	0.649
4	5000	0.9	40	1.190	0.524
5	3000	0.3	70	0.753	0.331
6	5000	0.3	70	0.655	0.304
7	3000	0.9	70	1.393	0.624
8	5000	0.9	70	1.117	0.504
9	2318	0.6	55	1.069	0.552
10	5682	0.6	55	0.818	0.349
11	4000	0.095	55	0.666	0.307
12	4000	1.105	55	1.535	0.654
13	4000	0.6	30	1.277	0.514
14	4000	0.6	80	0.806	0.36
15	4000	0.6	55	0.924	0.406
16	4000	0.6	55	0.923	0.413
17	4000	0.6	55	1.018	0.438
18	4000	0.6	55	0.898	0.392
19	4000	0.6	55	0.905	0.398
20	4000	0.6	55	0.979	0.425

Regression model for Taper:

$$\begin{aligned}
T = &\ 1.18095 - 0.000157604\,S - 0.127588\,F \\
&- 0.0123634\,P - 0.0000566667\,\text{SF} \\
&+ 0.00566667\,\text{FP} + 0.0000000175856\,S^2 \\
&+ 0.313247\,F^2 + 0.000056945\,P^2
\end{aligned} \tag{4}$$

3.2 ANOVA of regression models

After modeling the responses in terms of process variables, ANOVA was conducted on experimental data for its statistical validation. The details of ANOVA for CW and T are logged in Tables 5 and 6, respectively.

The experimental observations were validated in terms of various statistical attributes of ANOVA namely R^2,

Table 5 ANOVA for chipping width

Source	Sum of squares	Degree of freedom	Mean square	F value	P value	% Contribution
Model	1.16	7	0.17	68.28	< 0.0001	
S-speed	0.099	1	0.099	40.89	< 0.0001	8.32
F-feed	0.79	1	0.79	323.00	< 0.0001	66.39
P-power	0.16	1	0.16	67.34	< 0.0001	13.45
SF	0.018	1	0.018	7.46	0.0182	1.51
FP	0.019	1	0.019	7.86	0.0159	1.60
F^2	0.057	1	0.057	23.49	0.0004	4.79
P^2	0.025	1	0.025	10.45	0.0072	2.10
Residual	0.029	12	0.002431			
Lack of fit	0.018	7	0.002577	1.16	0.4516	
Pure error	0.011	5	0.002226			
Cor total	1.19	19				
R^2 97.55%	Adjusted R^2 96.12%		Predicted R^2 90.99%		Adequate precision 29.24	

Table 6 ANOVA for Taper

Source	Sum of squares	Degree of freedom	Mean square	F value	P value	% Contribution
Model	0.22	8	0.027	65.05	< 0.0001	
S-speed	0.035	1	0.035	84.68	< 0.0001	15.91
F-feed	0.14	1	0.14	326.54	< 0.0001	63.64
P-power	0.022	1	0.022	53.55	< 0.0001	10.00
SF	0.002312	1	0.002312	5.53	0.0384	1.05
FP	0.005202	1	0.005202	12.44	0.0047	2.37
S^2	0.004457	1	0.004457	10.66	0.0075	2.03
F^2	0.011	1	0.011	27.39	0.0003	5.00
P^2	0.002366	1	0.002366	5.66	0.0366	1.08
Residual	0.004600	11	0.0004182			
Lack of fit	0.003122	6	0.0005203	1.76	0.2758	
Pure error	0.001478	5	0.0002956			
Cor total	0.22	19				

| R^2 97.93% | Adjusted R^2 96.42% | | Predicted R^2 91.22% | | Adequate Precision 28.37 | |

predicted R^2, adjusted R^2, lack of fit and adequate precision. The R^2 (coefficient of determination) for CW and T were found as 97.55% and 97.93%, respectively. These high values, approaching the ideal value of 100%, explicate the capability of independent variables to explain the variance in output responses. However, larger value of R^2 should not be the sole criteria to interpret good approximation between the input variables and output responses. Adding a variable to the model always increases R^2 regardless of whether the additional variable is statistically significant or not. Accordingly, large number of variables usually led to higher R^2. Thus, it is desirable to look at adjusted R^2 and predicted R^2 statistics. The predicted R^2, 90.99% and 91.22%, for CW and T, respectively, were noticed to be adequately tuned with the corresponding adjusted R^2 values of 96.12% and 96.42%, which again validates the adequacy of developed models. Other than that the adequate precision, 29.24 and 28.37 for CW and T, respectively, was found higher than 4, which is desirable from statistical point of view [38–40]. The confidence level was kept 95% and accordingly the model terms having p values higher than 0.05 were treated as "insignificant." The "lack of fit" greater than 0.05 for CW and T models postulated another evidence of adequacy of regression models. Thereafter, sum of squares of individual term was divided by total sum of squares to find their relative contribution on responses of interest [41].

For confirmation of normal distribution of experimental data, normal plot of residuals were plotted for chipping width and taper as shown in Fig. 4. Residuals were found to scatter very close to the line of best fit, affirming the normal distribution of residuals [42]. Further, Fig. 5 also displays the fine tuning between the actual and predicted values of

Fig. 4 Normal plots for **a** CW and **b** T

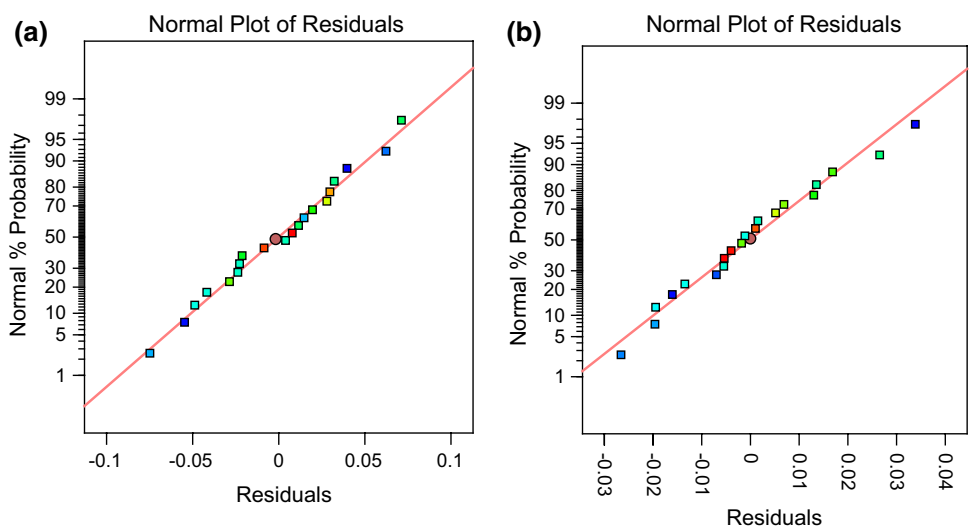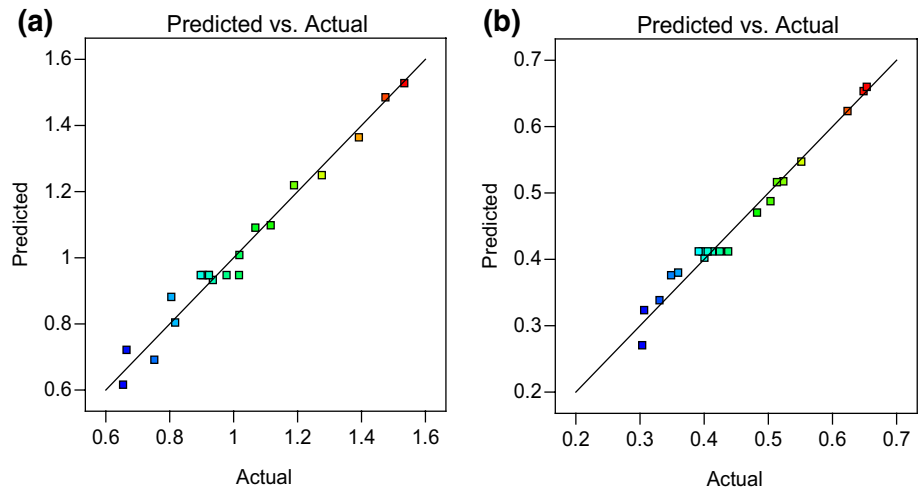**Fig. 5** Plot between actual and predicted results for **a** CW and **b** T

responses, which certified the high accuracy of regression models.

3.3 Effect of input variables on chipping width

ANOVA test on experimental observations of CW identified the significant model terms, which influence the CW. The significant terms are selected on the basis of their p value (less than or equal to 0.05), and their priority is decided on the basis of their percentage contribution. Except the second-order term of spindle speed and its interaction with power, all the remaining single-order, second-order and interaction terms of input variables were found significant.

To observe the variation in "chipping width" with change in input process parameters 3-dimensional surface plots were drawn that are shown in Fig. 6. Figure clearly shows that there is very steep increase in CW with small increase in feed. Highest level of feed 1.105 mm/min resulted in maximum chipping width of 1.535 mm as evidenced from 12th trial in Table 4. Percentage contribution in Table 5 shows that feed has monotonous effect on CW (66%) descended by ultrasonic power (13%) and spindle rpm (8%). This can be attributed to the fact that cutting forces are directly proportional to the feed rate [37–39]. Higher feed gives rise to higher stresses due to relatively smaller area of contact between workpiece and tool as the tool is hollow. Therefore, stress concentration occurs and results in easy propagation of cracks. Severe fracture takes place at higher feed as median cracks travel deeper into work surface. Consequently, larger chipping takes place. Moreover, at higher feed rate, distance covered by tool per unit time becomes higher that adds to
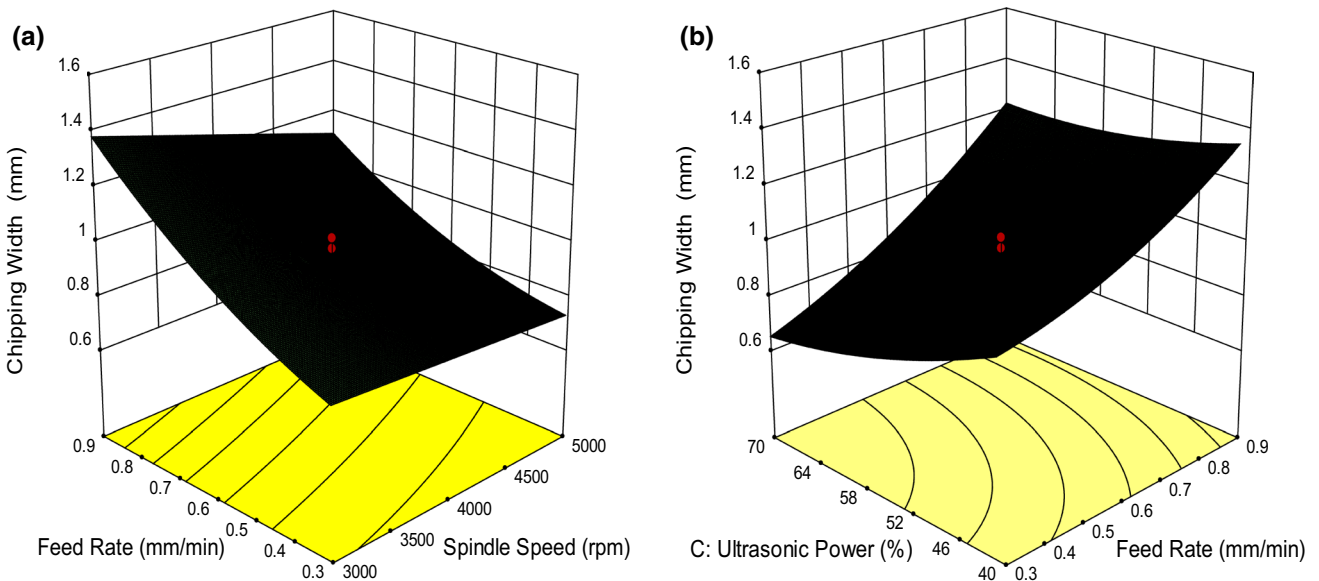

Fig. 6 3-D Surface plots for chipping width

the ultrasonic vibrations during their downward stroke. Consequently, the magnitude of impact of ultrasonic vibration increases sharply leading to severe knocking of workpiece. Due to high impact energy, the undrilled thickness of the workpiece undergoes severe brittle fracture resulting in high chipping damage.

CW decreases with increase in ultrasonic power because the increase in ultrasonic power decreases the cutting forces [38–40]. The decrease in cutting force can be attributed to increase in ultrasonic amplitude at higher power. Ultrasonic vibrations at higher amplitudes endorse effective hammering action resulting in nucleation of incipient cracks. Consequently, the propagation of these preexisting microcracks requires less effort under the subsequent hammering. So, higher amplitude easily cuts the pre-cracked surfaces leading to reduction in cutting force. On the other hand, low power yields higher cutting forces. In this condition, when tool advances in workpiece, the undrilled thickness (that decreases continuously with tool advancement) under tool tip finds it difficult to sustain these high forces. As a result, last few layers of workpiece are knocked-off suddenly under recurring ultrasonic vibrations. Therefore, it can be concluded that higher power levels effectively hinder the crack propagation and suppress the chipping width. In addition, ultrasonic power at higher levels showed superior performance when amalgamated with lower levels of feed as depicted in Fig. 6b. Interaction of higher levels of ultrasonic power at lower levels of feed produced superior results to suppress the CW, as this interaction can be expected to significantly increase cutting forces and stresses. This affirms the fact that the response does not solely depend upon the variation of an independent machining variable, but also gets affected by the levels of other variables.

CW also decreases with an increase in spindle speed as the cutting forces are inversely proportional to the spindle speed. This could be due to decrease in indentation depth at higher levels of rpm. Also, increase in spindle speed enhances the contact length (distance traveled by an abrasive, when in contact with the surface of work material) [43]. Accordingly, the probability of uniform load distribution, over the abrasives, becomes high, which leads to reduction in cutting forces and stress concentration. The synergetic effect of all these actions suppressed the chipping damage by reducing the cutting force with elevating RPM. Ning et al. also observed similar trends of reduced chipping damage [43]. Also, for interaction of spindle speed with higher feed rate, reduction in CW was more profound as compared to its interaction with lower feed as displayed in Fig. 6a.

3.4 Effects of input variables on taper

Except the interaction effect of speed with power, all other single-order, second-order and interaction terms of input variables were found significant. Again, the feed showed its dominating nature to affect the taper descended by spindle speed and power.

To observe the variation in "taper" with change in input process parameters, 3-dimensional surface plots were drawn that are shown in Fig. 7. Figure clearly shows that there is very steep upsurge in taper with very little increase in
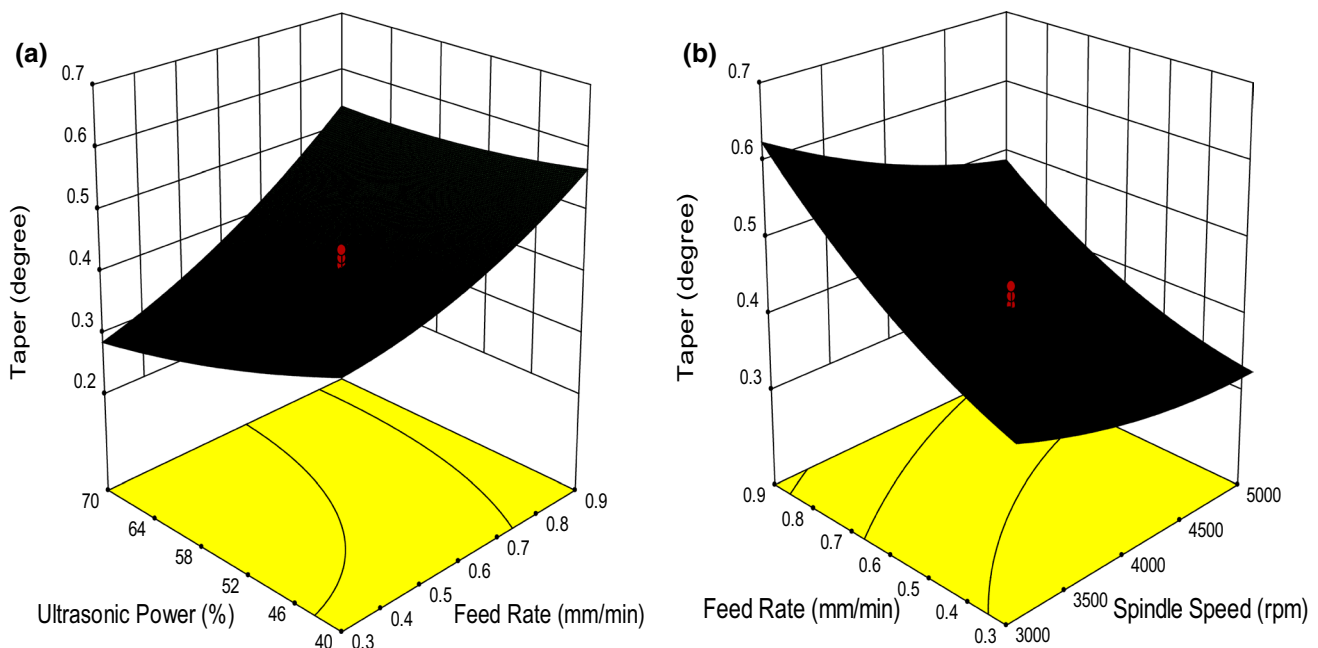

Fig. 7 3-D Surface plots for taper

feed. When tool touches the workpiece surface at the starting of drilling, there is a sudden change of drilling force from zero to maximum or near the maximum value. The value of maximum force increases continuously with increasing feed. Moreover, there is an intermittent contact of tool with workpiece as a consequence of ultrasonic vibrations. Taper is also reported to be directly correlated with surface roughness, i.e., taper increases with surface roughness [44]. In RUM, higher cutting forces result in the deeper indentation of abrasive into work surface leading to severe brittle fracture due to the generation of higher stresses. During its initial contact with workpiece, tool may also encounter transverse vibrations at micro level [45]. Under the combined effect of these conditions, hole diameter increases more than the desired value at the entry level.

After tool penetrates inside the work surface, drilling process becomes stable due to permanent contact and cutting forces show very little fluctuations [21, 46]. These fluctuations might be due to the concurrent occurrence of cutting and fracture of work surface. Also, the drilled hole starts to act like a jig to catch the transverse vibrations of tool. Therefore, hole size variation decreases as the tool penetrates deeper in glass surface. Simultaneous occurrence of all these events gives rise to higher taper at higher levels of feed.

From Fig. 7b, taper was found to lower down in a nonlinear fashion with increment in spindle rpm and power. One of the reasons for decrease in taper with increasing RPM is decrease in cutting forces. Higher rpm results in shallow indentation of abrasives. Consequently, material removal takes place in abrasion mode rather than extraction as in case of deep indentations of abrasives. Improvement in surface quality might also be expected due to lower forces and abrasion of workpiece surface. Because of reduced forces and better surface finish, taper was observed to decrease with increasing RPM.

Higher levels of ultrasonic power reduce taper which might be due to reduction in cutting forces and improvement in surface finish with continuous increase in power. Increasing power results in higher amplitudes of ultrasonic vibration. The working range of micro-grinding strokes among the abrasives coated on drill lateral surface and glass material is directly dependent on vibration amplitude. Accordingly, higher amplitude of ultrasonic vibration entails larger grinding strokes and generation of superlative surface finish. Some of the past studies also affirm the rise in grinding quality with elevation in vibration amplitude [47, 48]. All these conditions cause smaller deviations in hole diameter with tool advancement from hole entry side to exit size. So, higher levels of power can effectively reduce the taper. From Figs. 7a, b, it can be interpreted that the interactions of power with lower feed and higher speed bring about significant reduction in taper. This reduction can be attributed to

the fact that cutting forces are reduced with decrease in feed and increase in speed. These interactions were even more powerful in reducing the taper at higher levels of power as power increment also suppresses the forces.

3.5 Optimization through desirability

Often industrial problems involve more than one output responses that show different variations with change in input variables. Individually, each of these responses can be readily optimized. However, optimization becomes a cumbersome task when all of them have to be optimized concurrently. To deal with the complexity of simultaneous optimization of all the responses, researchers and process engineers commonly adopt "Desirability approach" [49]. The basic idea of desirability lies in finding those values of input variables, which assure compliance with the desired objectives of all the responses. For doing this, all the responses with their acceptable outcomes or desired goals are transformed into a single function known as the "desirability function." The value of desirability function is expressed in terms of composite desirability that is simply the geometric mean of desirability of individual responses. If all the goals of individual responses met their respective objectives or set goals, composite desirability is "1." If any of the considered response fails to meet the acceptable outcomes, desirability function tends to "zero."

The composite desirability (D) can be computed by the following equation:

$$D = \sqrt[n]{d_1^{w_1} \times d_2^{w_2} \times d_3^{w_3} \times \cdots \cdots \cdots \cdots \cdots \cdots \times d_n^{w_n}} \qquad (5)$$

where w is the weight of nth response; n is the total number of responses.

In Eq. 5 the composite desirability depends over few factors such as constraint imposed over input variables, nature of goals set for responses, weight and importance assigned to the responses. Weight allocated to response may have value from 0.1 to 10 and determines the shape of desirability function [50]. In the current study, weight of "1" was assigned to both the responses (CW and T) as it gives rise to linear variation in desirability function [39, 40]. Next step was to decide the criticalness of each response to allocate the suitable value of importance that ranges from 1 to 5. Both the responses were considered equally important. Accordingly, an unbiased value of 3 was assigned to responses as given in Table 7.

Final step is to determine the goals of input variables and output responses. There are different choices for setting the goal as "minimum," "maximum," "target" and none. The meaning and details of these goals are determined in Table 8.

Table 7 Constraints for desirability analysis

Process parameters	Units	Target	Lower bound	Upper bound	Weight	Importance
Feed	mm/min	In range	0.095	1.105	1	3
Spindle speed	RPM	In range	2318	5682	1	3
Ultrasonic Power	%	In range	30	80	1	3
CW	mm	Minimize	0.655	1.535	1	3
T	Degree	Minimize	0.304	0.654	1	3

Table 8 Meaning of desirability goals

Response objective/goal		
Maximum	Minimum	Target
$d_r = 0$ if $r < l_L$	$d_r = 1$ if $r < l_L$	$d_r = 0$ if $t_U < r < t_L$
$0 \le d_r \le 1$ as $l_L < r < u_L$	$0 \le d_r \le 1$ as $l_L < r < u_L$	$d_r = 1$ as $t_L < r < t_U$
$d_r = 1$ if $r > u_L$	$d_r = 0$ if $r > u_L$	

d_r response desirability, r response value, l_L lower acceptable limit of response u_L upper acceptable limit of response, t_U upper acceptable target value of response, t_L lower acceptable target value of response

If goal for any of the parameters is set "none," then that parameter is not included in the optimization process. To prevent the extrapolation (search of optimal solution outside design space), input variables were bound in their design limits with the goal "in range" as logged in Table 8. Extrapolation may have resulted into inaccurate solutions, as the process behavior is unknown outside the design space.

In the current study, CW and T were considered to evaluate the hole quality. Both CW and T are concerned with the qualitative aspect of drilled hole. So, both of them were optimized individually as well as simultaneously. Obviously, the objective of optimization was to minimize these responses. For individual optimization, when the desired goal is to minimize, the following equation is used to calculate the desirability (d_r) of response:

$$d_r = \left(\frac{u_L - r}{u_L - l_l} \right)^w \tag{6}$$

where u_L and l_L are upper and lower acceptable limits of response "r"; w: weight of response

For simultaneous optimization, Eq. 7 can be used to calculate the composite desirability and can be simplified as follows:

$$D = \sqrt{d_{CW}^{w_{CW}} \times d_T^{w_T}} \tag{7}$$

By using Eqs. 6 and 7, the optimal solutions were found corresponding to the situation where a single response has to be optimized as well as simultaneous optimization of responses. The optimal solutions for single response optimization and multi-response optimization have been given in Table 9. Despite the validation of prediction accuracy of response models through statistical analysis, two confirmation experiments were also conducted at the optimal settings. The average values of responses were compared with predicted values of response models. Confirmatory results have been summarized in Table 9. All the deviations between confirmation results and predicted results were found to lie within 5%, which validates the response models experimentally too.

The ramp function graph for selected optimal solution of multi-response optimization is shown in Fig. 8 with the composite desirability of output responses. The dot on the ramp for input variables shows the value that corresponds to the optimal solution. The height of dot indicates that how much desired it is. The location of the dot on the ramp for output response corresponds to the optimum value of the response [39]. Linear nature of ramp between the set boundaries and goal is due to assigning of equal weight to all the output responses and input variables.

Table 9 Optimal solutions for CW and T and validation results

Optimization	Response(s)	Optimized conditions			Predicted	Experimental	% Error
		Feed (mm/min)	Spindle speed (RPM)	Power (%)			
Single response	CW (mm)	0.19	5457	73	0.555	0.577	3.96
	T (degree)	0.11	5472	78	0.231	0.239	3.67
Multi-responses	CW (mm)	0.30	5000	70	0.615	0.641	4.22
	T (degree)				0.270	0.259	−4.07

(a) Spindle Speed = 5000   **(b)** Feed Rate = 0.3   **(c)** Ultrasonic Power = 70

Desirability = 1.000

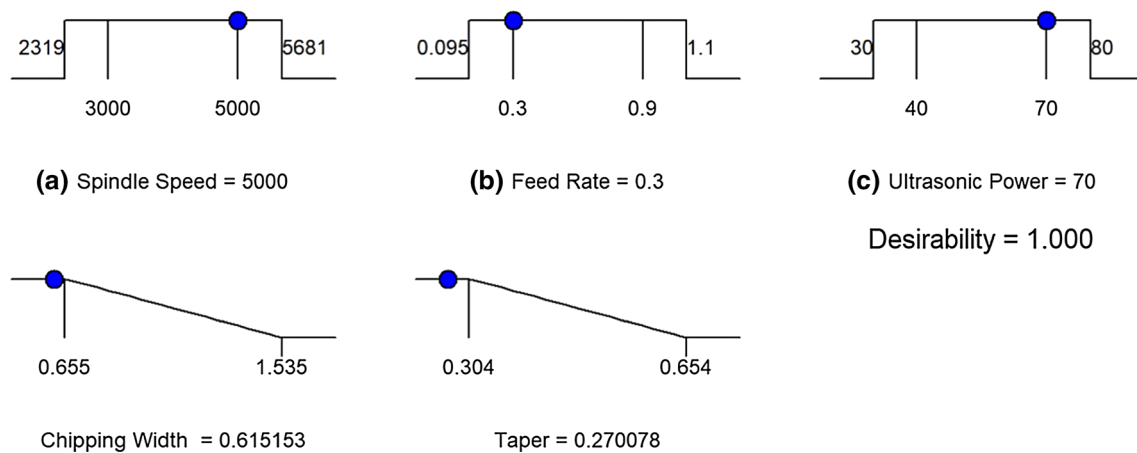Chipping Width = 0.615153   Taper = 0.270078

Fig. 8 Desirability ramp function graph for multi-response optimization (CW and T)
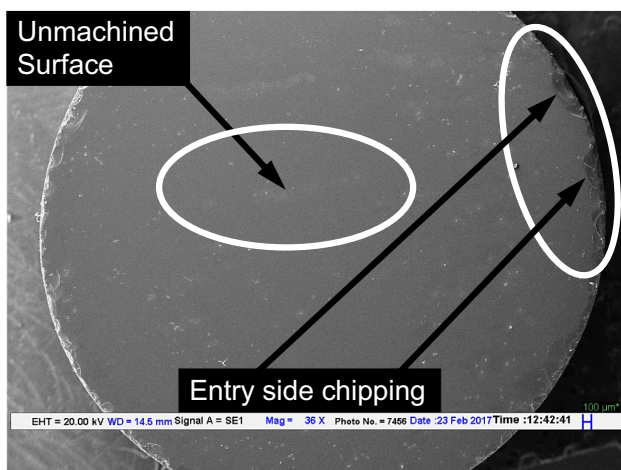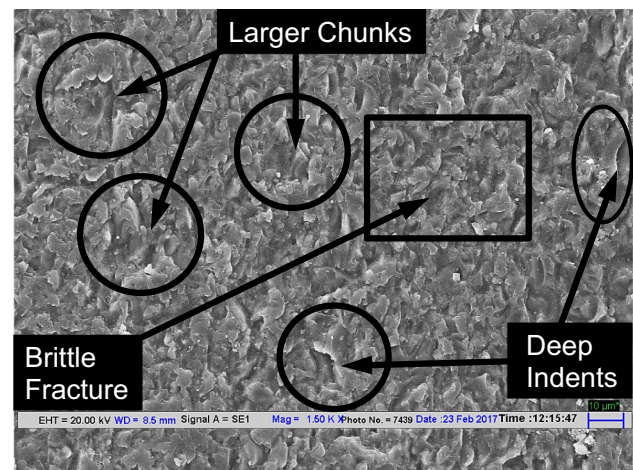

Fig. 9 Top view of machined rod

Fig. 10 Surface topography for experiment no. 7

3.6 Mechanism and microstructural analysis

In RUD, the trajectory of the diamond abrasive particle coated over the drill is the resultant of three different motions taking place concurrently. These three motions are:

1. Rotational motion of the spindle due to which abrasive particles move tangentially perpendicular to the tool axis
2. Ultrasonic vibration due to which abrasive particle reciprocate up and down
3. Downward axial feed of the diamond tool due to which abrasive moves in downward direction

The resultant of all the three motions appears in the form of spiral sinusoidal trajectory of abrasive particles. The material removal mechanism resembles the basic mechanism of the ultrasonic machining under combined effect of feed and ultrasonic vibration. But additional rotational motion transmitted by spindle to cutting drill makes the RUM superior and results in higher machining efficacy. The material in form of microchips is removed by hammering, abrasion and extraction in RUD [51].

Scanning electron microscope (SEM, EVO 18) was used to examine the topography of processed surface. Workpiece surface before machining and chipping damage at the top side of machined rod are depicted in Fig. 9. Figure 10 demonstrates the microstructure of machined surface for experiment no. 7 corresponding to feed of 0.90 mm/min. Higher feed promotes the deep penetration of abrasive into the workpiece. Further low rpm of 3000 generates high cutting forces. Amalgamation of higher feed and lower rpm resulted in the dominance of brittle fracture despite the high power of 70%. The reason might
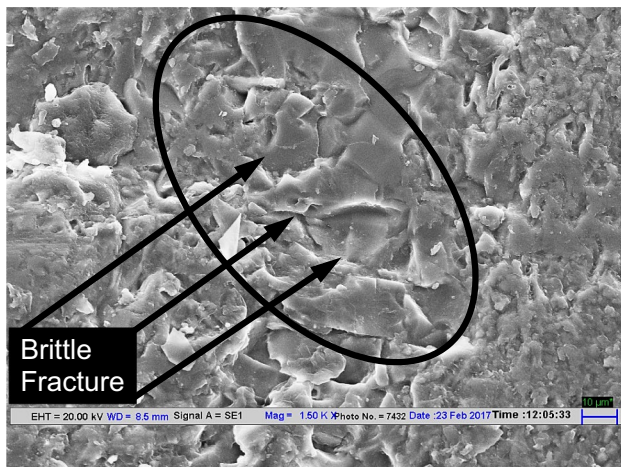
Fig. 11 Surface topography for experiment no. 12
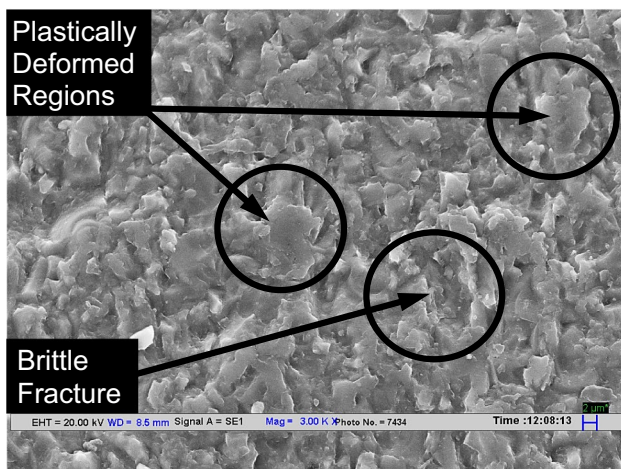

Fig. 12 Surface topography for experiment no. 6

be dominance of extraction mode of material removal over the abrasion mode due to high feed.

Figure 11 shows the SEM micrograph of machined surface corresponding to trial no. 12 at feed of 1.105 mm/min. Processed surface was found suffering from severe brittle fracture. Bigger and deep grooves were observed attributing to deep penetration at the highest level of feed. SEM micrograph in Fig. 12 for trial no.6 reveals the mixed flow of material at a feed rate of 0.30 mm/min in conjugation with 70% power at 5000 rpm. Lower feed gives rise to lower cutting forces. Moreover high power endorses better grinding, and high rpm causes uniform load distribution on abrasives. Accordingly plastically deformed regions were formed that are marked by circles.

3.7 Effect of backing plate

Before the main experimentation, pilot experimentation was conducted. Pilot experimentation not only helped to select the feasible range of significant process variables but also revealed the severe chipping damage at the hole exit. This damage needed a preventive measure for improving the machinability. In some of the studies, use of the backing material is reported to effectively reduce the edge chipping [7, 52]. Therefore, in present study, a soda lime glass plate of 12 mm thickness was placed beneath the workpiece sheet during the main experimentation to curb the chipping damage. Thereafter, a regression model (reported in Eq. 3) was developed to predict the chipping width at any combination of input variables. Confirmation experimentation (reported in Table 9) validated the high prediction accuracy of this model at 95% confidence level. Further, the results of pilot experimentation were compared with the values predicted by the CW model as expounded in Table 10. It should be noted that pilot experimentation was performed without using any backing plate. During the pilot experimentation, workpiece was supported over a fixture. The fixture was provided with different diameter holes. Hole of 14 mm diameter was selected for the pilot experimentation, and workpiece was clamped over fixture in such a manner that core drill is concentric with the fixture hole. This arrangement nullified the effect of backing support of fixture on the exit side chipping. For high precision, workpiece was clamped over fixture in such a manner that core drill is concentric with the fixture hole. Additionally, this arrangement resulted in the easy removal of machined rod that goes into fixture hole. Furthermore, it also avoided the tool hammering with metal fixture and prevented unnecessary tool wear and tool damage. The comparison between predicted values and experimental values in Table 10 is a concrete evidence of an effective reduction in chipping with backing the material being drilled. The approach of using backing plate resulted

Table 10 Comparison of predicted and experimental CW

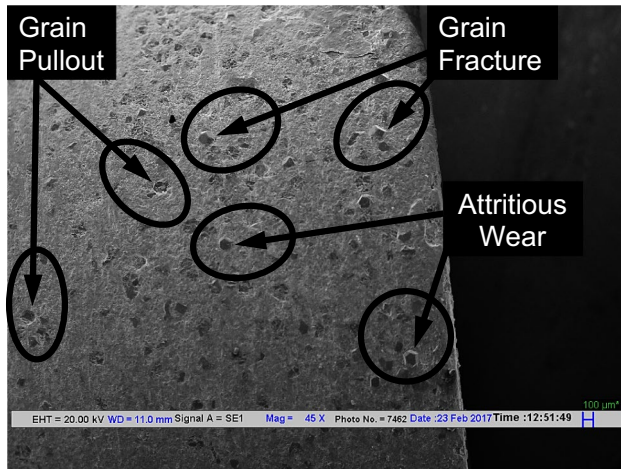| Spindle speed (RPM)	Feed (mm/min)	Ultrasonic power (%)	Predicted CW (mm)	Experimental CW (mm)	Reduction in CW (%)
2000	0.3	40	1.045	1.517	31.11
3000	0.3	40	1.007	1.383	27.19
4000	0.3	40	0.970	1.292	24.92
5000	0.3	40	0.932	1.169	20.27
3000	0.3	50	0.865	1.075	19.53
3000	0.3	60	0.759	0.941	19.34
3000	0.3	70	0.691	0.908	23.90
3000	0.6	40	1.183	1.631	27.47
3000	0.9	40	1.484	2.405	38.30

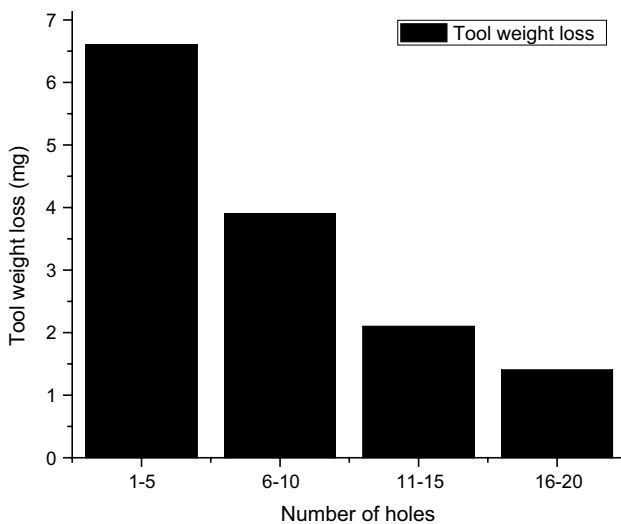**Fig. 13** Different types of tool wear

Fig. 14 Tool weight loss

in substantial reduction in chipping. This might be due to support by backing material to the undrilled thickness (thickness of workpiece that is yet to be drilled). Backing plate helped the workpiece to maintain its strength at the end of drilling to counteract the generated cutting forces through cushioning effect [7].

3.8 Tool wear

Scanning electron microscopic (SEM) image of tool lateral surface at 45×, shown in Fig. 13, is depicting the different modes of tool wear. Semi-micro weighing balance (GR-202, A&D Ltd.) has been used to measure the tool wear in terms of weight loss. An interval of five holes was chosen to measure the tool weight to shed more light on tool wear

trend. Overall 14 mg weight loss was observed for drilling 20 holes at different parametric conditions. 6.6 mg (47%) weight loss has been observed during the drilling of first five holes. It might be due to the dominance of grain fracture (partial breaking of abrasives) and bond fracture (complete dislodging of abrasive) in the initial stage of experimentation. The weight loss for next three set with an interval of five holes was 3.9 mg (27.86%), 2.1 mg (15%) and 1.4 mg (10%), respectively, as shown in Fig. 14. The decrease in the tool weight loss with proceeding experimentation is sharply reduced. It might be due to a reduction in grain fracture and bond fracture. Some of the weight loss in the later stage is attributed to attritious wear which refers to gradual blunting of cutting edges and making them flat. So, grain fracture and bond fracture contribute the major portion of tool weight loss whereas small contribution is made by attritious wear. Still, the tool wear in RUD remains less as compared to the conventional drilling due to the involvement of smaller cutting forces as a consequence of ultrasonic energy [53].

4 Conclusions

In this study, RUD of borosilicate glass has been performed with the objective of improving hole quality in context of process parameters "chipping width" and "taper." CCRD approach of RSM was used to plan the experimental scheme and modeling the process parameters. The key findings of experimental investigation can be listed as follow:

- The selected process parameters—feed rate, spindle speed and ultrasonic power—turned out to be significant in affecting the hole quality expressed in terms of taper and chipping width at the hole exit. Further high values of R^2 adjusted as 96.12 for chipping width and 96.42 for taper models suggest that process parameters and machining quality characteristics are strongly correlated.
- Chipping width and taper increased substantially with increasing feed, whereas both these quality characteristics were observed to decrease moderately with increasing spindle speed and power.
- Statistical analysis of experimental data using ANOVA inferred that the feed rate manifested the highest percentage contribution of 66.39% and 63.64% on chipping width and taper, respectively.
- The application of desirability approach for simultaneous optimization of both the responses yielded an optimal setting of speed as 5000 rev/min, feed rate as 0.30 mm/min and power as 70%. The values of chipping width and taper at the optimal setting were obtained as 0.641 mm

and 0.259 degree, respectively, based upon confirmation experiments.

- For individual optimization of chipping width to minimum value of 0.577 mm, the parametric combination emerged as feed 0.19 mm/min, spindle speed as 5457 rpm and power as 73%. Least taper of 0.239 was observed at feed 0.11 mm/min, spindle speed 5472 rpm and power 78%.

- The topographical study of processed surface using scanning electron microscope revealed that low feed, high rpm and high power have positive influence on the surface integrity due to mixed flow of material, whereas high feed, low speed and low power resulted in poor surface integrity due to complete dominance of brittle fracture. Higher levels of feed not only degraded the hole quality but also had obtrusive effect on surface integrity of processed surface due to formation of bigger and deep craters under severe brittle fracture.

- Use of backing plate resulted into significant reduction of chipping due to cushioning effect, which counteracted the cutting forces.

- SEM analysis revealed that tool encountered three kinds of wear—attritious wear, grain fracture and bond fracture. Further, measurement of loss of tool weight revealed that 47% of total weight loss occurred in the drilling of first five holes due to dominance of grain fracture and bond fracture. The weight loss for next three sets with an interval of five holes was 27.86%, 15% and 10% respectively.

Compliance with ethical standards

Conflict of interest The authors declare that they have no conflict of interest to report.

References

1. Barahimi V, Farahnakian M (2016) Experimental investigation of the surface roughness in grinding of BK7 optical glass in brittle mode. J Mod Process Manuf Prod 5:33–41
2. Huu Loc P, Shiou F, Yu Z, Hsu W (2013) Investigation of optimal air-driving fluid jet polishing parameters for the surface finish of N-BK7 optical glass. J Manuf Sci Eng 135:1–7. https://doi.org/10.1115/1.4023368
3. Kumar S, Singh AK (2017) Magnetorheological nanofinishing of BK7 glass for lens manufacturing. Mater Manuf Process 33:1188–1196. https://doi.org/10.1080/10426914.2017.1364759
4. Pal RK, Garg H, Sarepaka RV, Karar V (2016) Experimental investigation of material removal and surface roughness during optical glass polishing. Mater Manuf Process 31:1613–1620. https://doi.org/10.1080/10426914.2015.1103867
5. Liu D, Tang Y, Cong WL (2012) A review of mechanical drilling for composite laminates. Compos Struct 94:1265–1279. https://doi.org/10.1016/j.compstruct.2011.11.024
6. El-Hofy HA-G (2005) Advance machining processes. McGraw-Hill, New York
7. Hocheng H, Tsao CC (2005) The path towards delamination-free drilling of composite materials. J Mater Process Technol 167:251–264. https://doi.org/10.1016/j.jmatprotec.2005.06.039
8. Pei ZJ, Prabhakar D, Ferreira PM, Haselkorn M (1995) A mechanistic approach to the prediction of material removal rates in rotary ultrasonic machining. J Eng Ind 117:142–151. https://doi.org/10.1115/1.2803288
9. Cong WL, Feng Q, Pei ZJ et al (2012) Rotary ultrasonic machining of carbon fiber-reinforced plastic composites: using cutting fluid vs. cold air as coolant. J Compos Mater 46:1745–1753. https://doi.org/10.1177/0021998311424625
10. Lv D (2016) Influences of high-frequency vibration on tool wear in rotary ultrasonic machining of glass BK7. Int J Adv Manuf Technol 84:1443–1455. https://doi.org/10.1007/s00170-015-7204-1
11. Yadava V, Deoghare A (2008) Design of horn for rotary ultrasonic machining using the finite element method. Int J Adv Manuf Technol 39:9–20. https://doi.org/10.1007/s00170-007-1193-7
12. Kumaran ST, Ko TJ, Li C et al (2017) Rotary ultrasonic machining of woven CFRP composite in a cryogenic environment. J Alloys Compd 698:984–993. https://doi.org/10.1016/j.jallcom.2016.12.275
13. Jain AK, Pandey PM, Narasaiah K et al (2018) Effect of tool design parameters study in micro rotary ultrasonic machining process. Int J Adv Manuf Technol 98:1267–1285. https://doi.org/10.1007/s00170-018-2239-8
14. Sharma A, Jain V, Gupta D (2018) Characterization of chipping and tool wear during drilling of float glass using rotary ultrasonic machining. Measurement 128:254–263. https://doi.org/10.1016/j.measurement.2018.06.040
15. Song X, Yang J, Ren H et al (2018) Ultrasonic assisted high rotational speed diamond machining of dental glass ceramics. Int J Adv Manuf Technol 96:387–399. https://doi.org/10.1007/s00170-017-1571-8
16. Jain AK, Pandey PM (2018) Experimental studies on tool wear in μ-RUM process. Int J Adv Manuf Technol 85:2125–2138
17. Wang J, Feng P, Zhang J (2018) Reducing edge chipping defect in rotary ultrasonic machining of optical glass by compound step-taper tool. J Manuf Process 32:213–221. https://doi.org/10.1016/j.jmapro.2018.02.001
18. Lv D, Zhang Y, Peng Y (2016) High-frequency vibration effects on hole entrance chipping in rotary ultrasonic drilling of BK7 glass. Ultrasonics 72:47–56. https://doi.org/10.1016/j.ultras.2016.07.011
19. Alam K, Hassan E, Bahadur I (2015) Experimental measurements of temperatures in ultrasonically assisted drilling of cortical bone. Biotechnol Biotechnol Equip 29:753–757. https://doi.org/10.1080/13102818.2015.1034176
20. Mandegari M, Behbahani S (2013) Experimental analysis of a novel rotary ultrasonic assisted drilling (RUAD) machine. Mater Manuf Process 28:481–487. https://doi.org/10.1080/10426914.2012.727122
21. Feng Q, Cong WL, Pei ZJ, Ren CZ (2012) Rotary ultrasonic machining of carbon fiber-reinforced polymer: feasibility study. Mach Sci Technol 16:380–398. https://doi.org/10.1080/10910344.2012.698962

22. Churi NJ, Pei ZJ, Treadwell C (2006) Rotary ultrasonic machining of titanium alloy: effects of machining variables. Mach Sci Technol 10:301–321. https://doi.org/10.1080/10910340600902124

23. Zhao C-Y, Gong H, Fang FZ, Li ZJ (2013) Experimental study on the cutting force difference between rotary ultrasonic machining and conventional diamond grinding of K9 glass. Mach Sci Technol 17:129–144. https://doi.org/10.1080/10910344.2012.747930

24. Li Z, Zhang D, Jiang X et al (2017) Study on rotary ultrasonic-assisted drilling of titanium alloys (Ti6Al4 V) using 8-facet drill under no cooling condition. Int J Adv Manuf Technol 90:3249–3264. https://doi.org/10.1007/s00170-016-9593-1

25. Gupta V, Pandey PM (2016) An in vitro study of cutting force and torque during rotary ultrasonic bone drilling. Proc Inst Mech Eng Part B J Eng Manuf 232(9):1549–1560. https://doi.org/10.1177/0954405416673115

26. Yuan S, Zhu G, Zhang C (2017) Modeling of tool blockage condition in cutting tool design for rotary ultrasonic machining of composites. Int J Adv Manuf Technol 91:2645–2654. https://doi.org/10.1007/s00170-016-9911-7

27. Wang J, Feng P, Zhang J (2016) Investigations on the edge-chipping reduction in rotary ultrasonic machining using a conical drill. Proc Inst Mech Eng Part B J Eng Manuf 230:1254–1263. https://doi.org/10.1177/0954405416654426

28. Wang J, Feng P, Zheng J, Zhang J (2016) Improving hole exit quality in rotary ultrasonic machining of ceramic matrix composites using a compound step-taper drill. Ceram Int 42:13387–13394. https://doi.org/10.1016/j.ceramint.2016.05.095

29. Wang J, Feng P, Zhang J (2016) Reduction of edge chipping in rotary ultrasonic machining by using step drill: a feasibility study. Int J Adv Manuf Technol 87:2809–2819. https://doi.org/10.1007/s00170-016-8655-8

30. Wang J, Feng P, Zhang J et al (2016) Modeling the dependency of edge chipping size on the material properties and cutting force for rotary ultrasonic drilling of brittle materials. Int J Mach Tools Manuf 101:18–27. https://doi.org/10.1016/j.ijmachtools.2015.10.005

31. Cong WL, Pei ZJ, Treadwell C (2014) Preliminary study on rotary ultrasonic machining of CFRP/Ti stacks. Ultrasonics 54:1594–1602. https://doi.org/10.1016/j.ultras.2014.03.012

32. Hamzah E, Sudin I, Khoo C-Y, Abidin NNZ, Tan M-J (2008) Effect of machining parameters on BK7 optical glass using conventionaland rotary ultrasonic machines. J JSEM 8:127–132. https://doi.org/10.11395/jjsem.8.s127

33. Chen S, Jiang Z, Wu Y, Yang H (2011) Development of a grinding–drilling technique for holing optical grade glass. Int J Mach Tools Manuf 51:95–103. https://doi.org/10.1016/j.ijmachtools.2010.12.001

34. Santhanakrishnan M, Sivasakthivel PS, Sudhakaran R (2017) Modeling of geometrical and machining parameters on temperature rise while machining Al 6351 using response surface methodology and genetic algorithm. J Braz Soc Mech Sci Eng 39:487–496. https://doi.org/10.1007/s40430-015-0378-5

35. Sematech NIST (2006) Engineering statistics handbook. The National Institute of Standards and Technology (NIST)

36. Montgomery DC (2000) Design and analysis of experiments, 5th edn. Wiley, London

37. Ghodsiyeh D, Golshan A, Izman S (2014) Multi-objective process optimization of wire electrical discharge machining based on response surface methodology. J Braz Soc Mech Sci Eng 36(2):301–313. https://doi.org/10.1007/s40430-013-0079-x

38. Chittaranjandas V (2016) Response surface methodology and desirability approach to optimize EDM parameters. Int J Hybrid Inf Technol 9:393–406. https://doi.org/10.14257/ijhit.2016.9.4.34

39. Naresh Babu M, Muthukrishnan N (2014) Investigation on surface roughness in abrasive water-jet machining by the response surface method. Mater Manuf Process 29:1422–1428. https://doi.org/10.1080/10426914.2014.952020

40. Gopalakannan S, Senthilvelan T (2014) Optimization of machining parameters for EDM operations based on central composite design and desirability approach. J Mech Sci Technol 28:1045–1053. https://doi.org/10.1007/s12206-013-1180-x

41. Stalin John MR, Balaji B, Vinayagam BK (2017) Optimisation of internal roller burnishing process in CNC machining center using response surface methodology. J Braz Soc Mech Sci Eng 39:4045–4057. https://doi.org/10.1007/s40430-017-0871-0

42. Gurubasavaraju TM, Kumar H, Arun M (2017) Evaluation of optimal parameters of MR fluids for damper application using particle swarm and response surface optimisation. J Braz Soc Mech Sci Eng 39:3683–3694. https://doi.org/10.1007/s40430-017-0875-9

43. Ning FD, Cong WL, Pei ZJ, Treadwell C (2016) Rotary ultrasonic machining of CFRP: a comparison with grinding. Ultrasonics 66:125–132. https://doi.org/10.1016/j.ultras.2015.11.002

44. Lalchhuanvela H, Doloi B, Bhattacharyya B (2013) Analysis on profile accuracy for ultrasonic machining of alumina ceramics. Int J Adv Manuf Technol 67:1683–1691. https://doi.org/10.1007/s00170-012-4601-6

45. Adithan M, Venkatesh VC (1976) Production accuracy of holes in ultrasonic drilling. Wear 40:309–318. https://doi.org/10.1016/0043-1648(76)90122-8

46. Churi N, Pei ZJ, Shorter D, Treadwell C (2009) Rotary ultrasonic machining of dental ceramics. Int J Mach Mach Mater 6:270–284. https://doi.org/10.4028/www.scientific.net/MSF.532-533.361

47. Zhang C, Cong W, Feng P, Pei Z (2014) Rotary ultrasonic machining of optical K9 glass using compressed air as coolant: a feasibility study. Proc Inst Mech Eng Part B J Eng Manuf 228:504–514. https://doi.org/10.1177/0954405413506195

48. Wang J, Feng P, Zhang J et al (2017) Investigations on the critical feed rate guaranteeing the effectiveness of rotary ultrasonic machining. Ultrasonics 74:81–88. https://doi.org/10.1016/j.ultras.2016.10.003

49. Sharma V, Kumar V (2016) Multi-objective optimization of laser curve cutting of aluminium metal matrix composites using desirability function approach. J Braz Soc Mech Sci Eng 38:1221–1238. https://doi.org/10.1007/s40430-016-0487-9

50. Dolado P, Lazaro A, Delgado M et al (2015) An approach to the integrated design of PCM-air heat exchangers based on numerical simulation: a solar cooling case study. Resources 4:796–818. https://doi.org/10.3390/resources4040796

51. Pei Z, Ferreira P, Kapoor S, Haselkorn M (1995) Rotary ultrasonic machining for face miling of ceramics. Int J Mach Tools Manuf 35:1033–1046. https://doi.org/10.1016/0890-6955(94)00100-X

52. Fernando PKSC, Pei Z, Zhang MP, Song X (2017) Rotary ultrasonic drilling of CFRP: effect of process parameters on delamination. In: Proceedings of ASME 2016 international manufacturing science and engineering conference, pp 1–6

53. Li Z, Zhang D, Qin W, Geng D (2017) Feasibility study on the rotary ultrasonic elliptical machining for countersinking of carbon fiber–reinforced plastics. Proc Inst Mech Eng Part B J Eng Manuf 231:2347–2358. https://doi.org/10.1177/0954405415626086